Title

Photodissociation of CO 2 between 13.540 eV and 13.678 eV

Journal

Physical Chemistry Chemical Physics, 16(2)

ISSN

0956-5000

Authors

Song, Yu
Gao, Hong
Chang, Yih Chung
et al.

Publication Date

2014-01-14

DOI

10.1039/c3cp53250j

Peer reviewed

PCCP

PAPER

View Article Online
View Journal | View Issue

Cite this: *Phys. Chem. Chem. Phys.*, 2014, **16**, 563

Photodissociation of CO_2 between 13.540 eV and 13.678 eV

Yu Song, Hong Gao,† Yih Chung Chang, Zhou Lu, C. Y. Ng* and William M. Jackson*

Received 1st August 2013,
Accepted 7th October 2013

DOI: 10.1039/c3cp53250j

www.rsc.org/pccp

Photodissociation of CO_2 is investigated between 13.540 eV and 13.678 eV using the time-sliced velocity-mapped ion imaging (TSVMI) apparatus that is combined with one-color and two-color pump–probe VUV + VUV and VUV + UV detection schemes by probing oxygen fragments at different levels. Several CO_2 dissociation channels are directly observed from the ion images, namely CO(X $^1\Sigma^+$) + O(^{1}D), CO(X $^1\Sigma^+$) + O(^{1}S), CO(a $^3\Pi$) + O(^{3}P), CO(a $^3\Pi$) + O(^{1}D), CO(a′ $^3\Sigma^+$) + O(^{3}P), CO(d $^3\Delta$) + O(^{3}P) and CO(e $^3\Sigma^-$) + O(^{3}P), whereas no CO(X $^1\Sigma^+$) + O(^{3}P) production has been found. The product kinetic energy distributions of these channels are reported for the first time. Possible dissociation mechanisms have been discussed based upon the product vibrational and rotational distributions.

1 Introduction

CO_2 is the major component in the atmospheres of Mars and Venus (>95% by volume), and it is also found in comets and the interstellar medium with relatively high abundance.[1] In addition, carbon dioxide in the Earth's atmosphere plays an important role as greenhouse gas that is increasing the average temperature due to anthropomorphic causes. Spectroscopic studies showed that CO_2 has a strong and broad absorption peak between 13 eV and 14 eV,[2] which corresponds to the transitions of numerous Rydberg states converging to the ground state of CO_2^+. Previous studies[3] showed that nearly 100% CO_2 will dissociate in this energy region. The energetically allowed channels from photodissociation of CO_2 below 14 eV to produce CO and O are listed here:[4]

$$CO_2 + h\nu \rightarrow CO(X\ ^1\Sigma^+) + O(^3P) \quad h\nu \geq 5.45\ \text{eV} \quad (1)$$

$$CO_2 + h\nu \rightarrow CO(X\ ^1\Sigma^+) + O(^1D) \quad h\nu \geq 7.42\ \text{eV} \quad (2)$$

$$CO_2 + h\nu \rightarrow CO(X\ ^1\Sigma^+) + O(^1S) \quad h\nu \geq 9.64\ \text{eV} \quad (3)$$

$$CO_2 + h\nu \rightarrow CO(a\ ^3\Pi) + O(^3P) \quad h\nu \geq 11.46\ \text{eV} \quad (4)$$

$$CO_2 + h\nu \rightarrow CO(a\ ^3\Pi) + O(^1D) \quad h\nu \geq 13.43\ \text{eV} \quad (5)$$

$$CO_2 + h\nu \rightarrow CO(a'\ ^3\Sigma^+) + O(^3P) \quad h\nu \geq 12.31\ \text{eV} \quad (6)$$

$$CO_2 + h\nu \rightarrow CO(d\ ^3\Delta) + O(^3P) \quad h\nu \geq 12.97\ \text{eV} \quad (7)$$

$$CO_2 + h\nu \rightarrow CO(e\ ^3\Sigma^-) + O(^3P) \quad h\nu \geq 13.35\ \text{eV} \quad (8)$$

$$CO_2 + h\nu \rightarrow CO(A\ ^1\Pi) + O(^3P) \quad h\nu \geq 13.48\ \text{eV} \quad (9)$$

$$CO_2 + h\nu \rightarrow CO(I\ ^1\Sigma^-) + O(^3P) \quad h\nu \geq 13.45\ \text{eV} \quad (10)$$

$$CO_2 + h\nu \rightarrow CO(D\ ^1\Delta) + O(^3P) \quad h\nu \geq 13.56\ \text{eV} \quad (11)$$

The photodissociation of CO_2 has been studied extensively during the last several decades. In 1972, Lawrence[3] measured the cross-section for the emission of the CO(a $^3\Pi$ – X $^1\Sigma^+$) Cameron bands produced from the photodissociation of CO_2 between 85 and 109 nm (11.375–14.587 eV), and found that the CO Cameron quantum yield increases smoothly and monotonically with the excitation energy of CO_2, reaching a maximum of 50–60% around 90 nm (13.777 eV). The production yield for the Cameron bands also includes the higher triplet states of CO(a′ $^3\Sigma^+$, d $^3\Delta$, e $^3\Sigma^-$) that can cascade through radiative decay to CO(a $^3\Pi$). The production of CO(a′ $^3\Sigma^+$, d $^3\Delta$, e $^3\Sigma^-$) from photodissociation of CO_2 at 76.4–92.3 nm (13.434–16.229 eV) was then confirmed[5] by observing the fluorescence from CO(a′ $^3\Sigma^+$, d $^3\Delta$, e $^3\Sigma^-$) to CO(a $^3\Pi$). He determined the cross-sections for the production of CO(a′ $^3\Sigma^+$, d $^3\Delta$, e $^3\Sigma^-$) from this fluorescence at 92.3 nm (13.434 eV) and 90.1 nm (13.762 eV) as 25 Mb and 10 Mb, respectively. Around 90 nm (13.777 eV) he observed that the spin-forbidden dissociation channel, (9) CO(A $^1\Pi$) + O(^{3}P), occurred by measuring the cross-section for the production of the CO fourth positive band fluorescence A $^1\Pi$ – X $^1\Sigma^+$ as 1–2 Mb. Later, Lawrence[6] showed by detection of the oxygen green line that ~30% CO_2 dissociates through channel (3) to produce O(^{1}S) atoms around 90 nm (13.777 eV). Recently, our group[7] reported the observation of channel (2) from photodissociation of CO_2 at O(^{1}D) autoionization line at 13.45 eV. In summary, the CO_2 dissociation channels (2)–(9) have been observed experimentally at ~90 nm (13.777 eV). Meanwhile, the potential energy surfaces for the first six singlet electronic states of CO_2 have

Department of Chemistry, University of California, Davis, CA 95616, USA.
E-mail: cyng@ucdavis.edu, wmjackson@ucdavis.edu
† Present address: Department of Chemistry, Stanford University, Stanford, CA 94305 USA.

been calculated by Grebenshchikov[8] using high level *ab initio* methods. These states are the adiabatic 1–3 $^1A'$ and 1–3 $^1A''$, which are found to strongly interact at avoided crossings and true intersections. A theoretical UV absorption spectrum of CO_2 was calculated using these theoretical potential energy surfaces for the five singlet valence states at 120–160 nm (7.750–10.333 eV)[9] that is in good agreement with the experimental spectrum[10] of CO_2 in this region. The interactions between the valence and Rydberg states were also discussed by calculating the first ten states of CO_2 at 0–12 eV, *i.e.*, 1–5 $^1A'$ and 1–5 $^1A''$.

In the current study, photodissociation of CO_2 is investigated between 13.540 eV and 13.678 eV by using the time-sliced velocity-mapped ion imaging (TSVMI) apparatus combined with two-color VUV + VUV and VUV + UV radiation. Dissociation channels (2)–(8) are directly observed from the sliced images, along with their translational energy distributions. The structures observed in the translational distributions are assigned to the internal product distributions of the energetically available channels. Little evidence has been found for the production of the lowest energy spin-forbidden dissociation channel, (1). Possible dissociation mechanisms have been derived from the product vibrational and rotational distributions, and predissociations between the initially excited Rydberg states and highly internally-excited lower-lying states have been found to be important during the CO_2 dissociation.

2 Experimental

The present study employs the time-sliced velocity-mapped ion imaging (TSVMI) apparatus combined with two-color VUV radiations that have been previously described,[11–13] so only a brief summary is provided. A pulsed molecular beam of pure CO_2 gas (Praxair, 99.5%) is generated by supersonic expansion through an Even–Lavie valve (EL-5-2004, nozzle diameter 0.2 mm) operating at 30 Hz with a stagnation pressure of 30 psi. The beam is collimated using two conical skimmers prior to entering the interaction region along the axis of velocity-mapped ion imaging optics, where it is crossed with two perpendicular VUV + VUV or VUV + UV beams that are counter-propagating to each other. In the present study, both one-color and two-color experiments have been carried out. One-color experiments use one single-frequency VUV radiation to photodissociate CO_2 and photoionize the fragment $O(^1S)$ atom, while in the two-color experiments one VUV radiation is used to photodissociate CO_2 and the other unfocused VUV or focused UV radiation to state-selectively ionize the $O(^1D)$ or $O(^3P)$ fragment, respectively. Both of the tunable VUV beams are generated by resonant four-wave mixing (RFWM) and produce VUV light at sum-frequency $2\omega_1 + \omega_2$ using Kr gas as the nonlinear medium.[14,15] The ω_1 represents the two-photon resonant frequency of Kr at 212.556 nm, which coincides with the Kr two-photon transition $4s^24p^5(^2P^o_{3/2})5p\ ^2[1/2]_0 \leftarrow 4s^24p^6\ ^1S_0$. The ω_2 represents the frequency of a tunable dye laser. The typical delay time between the dissociation and the probe source is 10–20 ns. The ions formed in the interaction region are accelerated by the ion imaging optics and then strike a dual microchannel plate (MCP) detector after travelling down a 75 cm flight tube. A high voltage pulse is applied to the front MCP at the expected arrival time for the fragment ion under observation, while the back one is set at +1100 V. The electrons from MCP hit a phosphor screen and the resulting image is recorded by a CCD camera and accumulated in a computer. Another detection strategy is the measurement of the photofragment yield spectrum where a −1400 V is put on the front of the MCP and the back of the MCP is grounded. The MCP signals are amplified and fed into both a digital oscilloscope and a boxcar integrator. A gate from the boxcar integrator is used to select the ion corresponding to a particular mass and to record this signal, while the photodissociation wavelength is scanned simultaneously.

3 Results and discussions

The aim of the present research is to directly confirm CO + O channels (1)–(11), in the photolysis of CO_2 in 13.540–13.678 eV VUV region by observing the sliced images of the oxygen $O(^3P_J)$, $O(^1D)$ and $O(^1S)$ fragments. Other channels such as $C + O_2$[16] will not be considered in the present work.

3.1 Detection of $O(^3P)$

Most of the dissociation channels, *i.e.*, (1), (4), (6)–(11), produce the $O(^3P)$ fragment, so by detecting this fragment we should be able to obtain information about the internal energy of the CO fragment. The current study employed a previously used 2 + 1 REMPI scheme to probe three spin–orbit components of $O(^3P)$ at 225.655 nm, 226.058 nm and 226.234 nm for J = 2, 1 and 0 levels, respectively.[17] Images are taken under different experimental conditions to confirm that the signal is due to the $O(^3P_J)$ fragment from the VUV photodissociation of CO_2. First, both dissociation VUV and probe UV beams are present in the interaction region, second, the dissociation beam is present while the probe beam is blocked, and third, the dissociation beam is blocked and the probe beam is present. The background images under conditions two and three are very weak compared to the image when both beams are present in the interaction region, and they have been subtracted from the image under condition one. Three TSVMI images that result from probing the different spin–orbit states of $O(^3P)$ at a photodissociation wavelength 91.15 nm (13.604 eV) are shown in Fig. 1(a)–(c). The total kinetic energy release (TKER) distributions derived from these images are shown in Fig. 1(d)–(f). A closer analysis reveals that all three images have similar patterns, with four weak circles on the outside and a brighter donut-shaped signal on the inside. The four circles in these images are assigned to the vibrationally-resolved CO($a\ ^3\Pi$, v = 0–3) + $O(^3P)$. The inner donut-shaped image is assigned to three unresolved spin-allowed channels CO($a'\ ^3\Sigma^+$) + $O(^3P)$, CO($d\ ^3\Delta$) + $O(^3P)$ and CO($e\ ^3\Sigma^-$) + $O(^3P)$. Fig. 1(d)–(f) show that the four circles corresponding to the vibrational progression of CO($a\ ^3\Pi$) from 1.3 eV to 2.2 eV and the sharp rising signal at 1.3 eV agree with

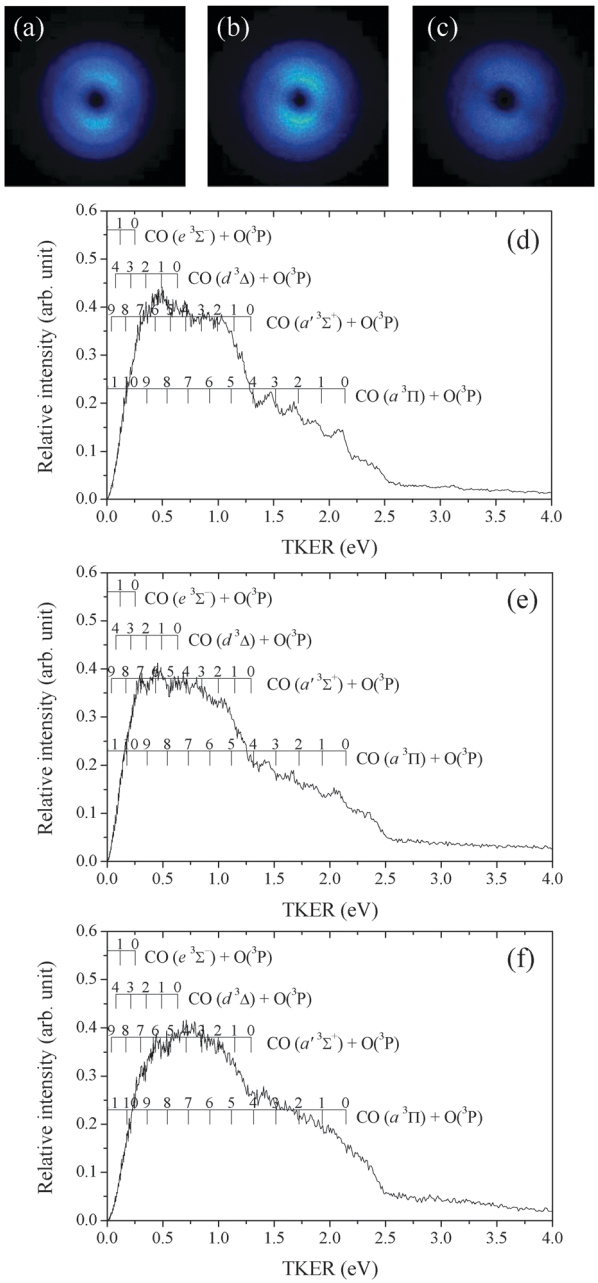

Fig. 1 Time-sliced velocity-mapped raw images of (a) O(^{3}P$_2$), (b) O(^{3}P$_1$), (c) O(^{3}P$_0$) and the total kinetic energy release (TKER) spectrum of the photofragments CO and O from photodissociation of CO_2 by detecting (d) O(^{3}P$_2$), (e) O(^{3}P$_1$), (f) O(^{3}P$_0$) at 13.604 eV. The vibrational assignments for the CO product at different electronically excited states are referring to CO at the ground rotational state J = 0. The same is true for the other figures.

the energies associated with the suggested product assignments fairly well for the dissociation of CO_2.

The ground and spin-forbidden dissociation channel CO(X $^1\Sigma^+$) + O(^{3}P) participates very little in the current dissociation region, as reflected by the dark area outside the four rings in the images and the weak signal beyond 2.5 eV in the TKER spectra. A small amount of the signal appears beyond the threshold of the lowest spin-allowed channel CO(a $^3\Pi$) + O(^{3}P) at 2.15 eV. This part of the signal is related to the VUV dissociation beam, since it will shift to higher kinetic energy in the TKER spectra accordingly with the increased VUV excitation energy. The same is true for the vibrationally-resolved CO(a $^3\Pi$, v = 0–3) + O(^{3}P) peaks and unresolved signal from 0 to 1.3 eV. We speculate that a small amount of the CO_2 molecules will absorb both the dissociation VUV photon at 13.604 eV and the probe UV photon at 5.49 eV, followed by its fragmentation to O(^{3}P) and a highly electronically excited CO molecule, which causes the weak signal beyond the threshold of CO(a $^3\Pi$) + O(^{3}P) at 2.15 eV. The signal-to-noise ratio is low for O(^{3}P$_0$) because of the smaller production of O(^{3}P$_0$) than O(^{3}P$_2$) and O(^{3}P$_1$). This suggests that the oxygen spin–orbit states are being produced with a statistical distribution as one would expect for dissociation that involves predissociation or internal conversion.[17]

The signal in TKER spectra from 0 eV to 2.2 eV contains multiple dissociation channels, namely CO(a $^3\Pi$, v = 0–10) + O(^{3}P), CO(a′ $^3\Sigma^+$, v = 0–8) + O(^{3}P), CO(d $^3\Delta$, v = 0–4) + O(^{3}P) and CO(e $^3\Sigma^-$, v = 0, 1) + O(^{3}P). It is possible that higher energetically-allowed channels CO(A $^1\Pi$) + O(^{3}P), CO(I $^1\Sigma^-$) + O(^{3}P) and CO(D $^1\Delta$) + O(^{3}P) are involved during the dissociation. However, their intensities are probably very small compared to those of the spin-allowed channels described above, since the TKER signal drops dramatically at the kinetic energy region from 0.15 eV to 0 eV.

The energy resolution of the TKER spectra is not high enough to clearly separate the dissociation pathways to the different electronic states of CO. Thus, we cannot use the TKER spectra to measure the branching ratios. There are currently no theoretical treatments that could be used to analyze these curves because this requires accurate potential energy curves in this energy region that are not available. Nevertheless, from the sharp steps at 1.3 eV in these TKER spectra, it is easy to point out that the production of CO(a′ $^3\Sigma^+$) + O(^{3}P) competes with that of CO(a $^3\Pi$) + O(^{3}P). No such steps have been found for the higher channels CO(d $^3\Delta$) + O(^{3}P) and CO(e $^3\Sigma^-$) + O(^{3}P), but these two channels cannot be excluded from the total CO_2 photodissociation production since the product CO(a′ $^3\Sigma^+$) vibrational distribution is unclear. The branching ratio between CO(a $^3\Pi$, v = 0–3) + O(^{3}P) and the rest of the possible pathways in Fig. 1(d)–(f), *i.e.*, CO(a $^3\Pi$, v = 4–10) + O(^{3}P), CO(a′ $^3\Sigma^+$, v = 0–8) + O(^{3}P), CO(d $^3\Delta$, v = 0–4) + O(^{3}P) and CO(e $^3\Sigma^-$, v = 0, 1) + O(^{3}P), is estimated to be 1 : 2.5 at 13.604 eV for all three spin–orbit components of O(^{3}P).

These results differ from the previous study by Judge and Lee,[5] in which the cross-sections for the production of CO(a′ $^3\Sigma^+$, v = 5–11), CO(d $^3\Delta$, v = 1–6) and CO(e $^3\Sigma^-$, v = 3) were measured for incident photons at 13.77 eV and 13.45 eV by the fluorescence from these states to CO(a $^3\Pi$). At 13.45 eV, the cross-section for the production of CO(a′ $^3\Sigma^+$, v = 5–8) and CO(d $^3\Delta$, v = 1–3) is 10.29 Mb and 15.39 Mb, respectively, and the most excited vibrational state is v = 5 for the former and v = 2 for the latter. At 13.77 eV, the cross-section for CO(a′ $^3\Sigma^+$, v = 5–11) is 3.5 Mb while for CO(d $^3\Delta$, v = 1–6) it is 6.93 Mb, and the most excited vibrational state is v = 7 and v = 2, respectively. The CO(e $^3\Sigma^-$, v = 3) cross-section is 0.07 Mb at 13.77 eV. At both wavelengths, the CO(a $^3\Pi$) yield is indicated to be small,

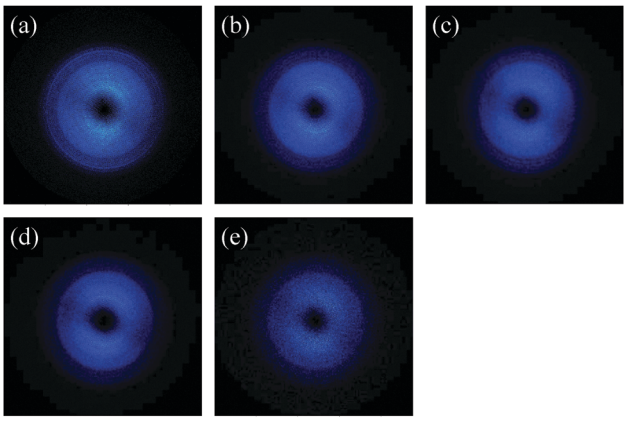

Fig. 2 Time-sliced velocity-mapped raw images of $O(^3P_2)$ from photodissociation of CO_2 at (a) 13.540 eV, (b) 13.549 eV, (c) 13.604 eV, (d) 13.612 eV, and (e) 13.620 eV.

as well as CO(a′ $^3\Sigma^+$, $v < 5$) and CO(d $^3\Delta$, $v = 0$). It should be noted that CO(a′ $^3\Sigma^+$, $v < 5$) and CO(d $^3\Delta$, $v = 0$) could not be detected in Judge and Lee's work,[5] since the fluorescence of these states populates at the undetected IR region (>800 nm). Meanwhile, the present data points out that the CO(a $^3\Pi$, $v = 0$–3) + $O(^3P)$ yield is about 30% in the total CO_2 dissociation production, and the step at 1.3 eV in the TKER spectra clearly illustrates the production of large amounts of CO(a′ $^3\Sigma^+$, $v = 0$–3), in contrast to the above assumptions. Although the fragment CO vibrational distribution could not be determined at this time, the TKER spectra shows that the CO(d $^3\Delta$) yield may not be as significant as previously proposed.[5]

Several $O(^3P_2)$ images have been collected at different CO_2 dissociation energies at 13.540 eV, 13.549 eV, 13.604 eV, 13.612 eV, and 13.620 eV, and they are shown in Fig. 2(a)–(e). All the images are similar to that at 13.604 eV in Fig. 1(a)–(c), except for the image at 13.540 eV in Fig. 2(a), which exhibits a sharp and bright ring at a larger radius. Fig. 3(a)–(c) are the TSVMI images for the photodissociation of CO_2 at 13.540 eV by probing $O(^3P_{2,1,0})$, while Fig. 3(d) and (e) are their related TKER spectra. The bright ring in Fig. 3 is revealed to be associated with CO(a $^3\Pi$, $v = 1$), which has a stronger distribution than CO(a $^3\Pi$, $v = 0, 2, 3$) for all three $O(^3P_2)$ spin–orbit fine structures. The relative amount of the CO(a $^3\Pi$, $v = 1$) compared to the CO(a $^3\Pi$, $v = 0, 2, 3$) states appears to decrease as one goes from $J = 2$ to $J = 0$. One possible explanation for the CO(a $^3\Pi$, $v = 1$) abnormal intensity is that around 13.540 eV one has the highest probability to cross over to the state that leads to CO(a $^3\Pi$, $v = 1$) + $O(^3P)$ final product. This part of the dissociation of CO_2 is so fast that after the dissociation the available energy could not be distributed evenly among all of the available vibrational degrees of freedom and oxygen spin–orbit states. This makes the CO(a $^3\Pi$) + $O(^3P)$ product channels non-statistical in the vibrational degrees of freedom.

The rotational distributions of CO(a $^3\Pi$, $v = 0$–3) are narrow and appear to peak at 400–500 cm^{-1} (derived from the difference between each peak in TKER spectrum and its corresponding vibrational assignment at rotational level $J = 0$) at all of the

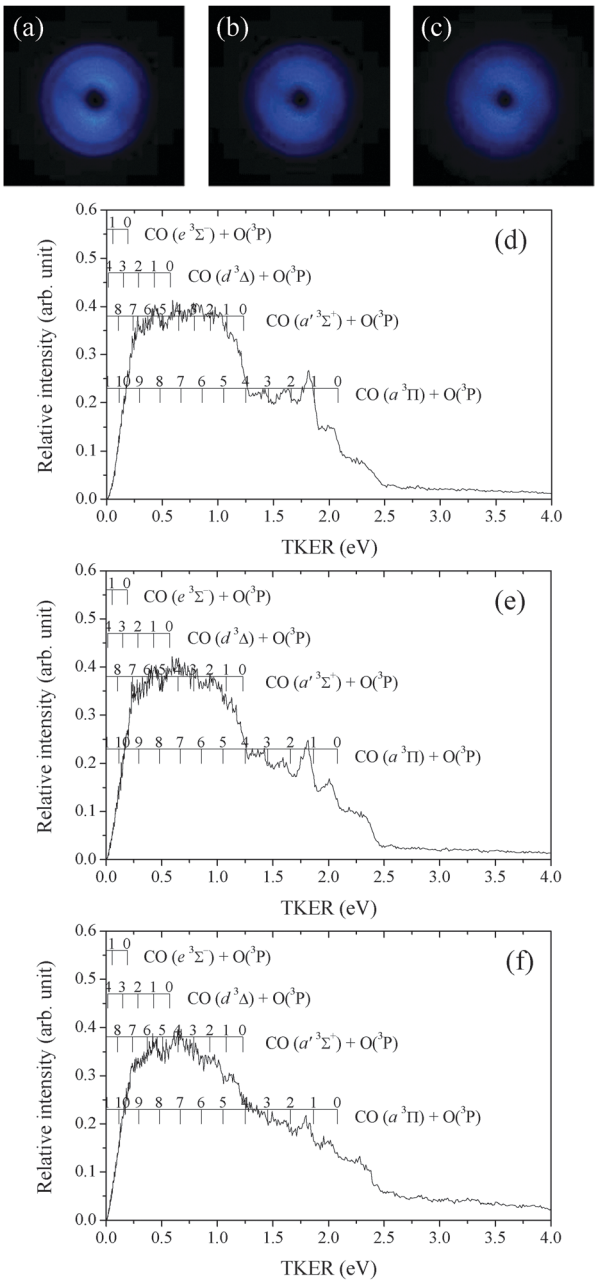

Fig. 3 Time-sliced velocity-mapped raw images of (a) $O(^3P_2)$, (b) $O(^3P_1)$, (c) $O(^3P_0)$ and the total kinetic energy release (TKER) spectrum of the photofragments CO and O from photodissociation of CO_2 by detecting (d) $O(^3P_2)$, (e) $O(^3P_1)$, (f) $O(^3P_0)$ at 13.540 eV.

investigated wavelengths. This cold product rotational temperature indicates that the bending motion of the CO_2 molecule is not extensively excited along the dissociation coordinate and the dissociating CO_2 molecule probably possesses a near linear geometry. The anisotropy parameter β is 0.2–0.4 for all the dissociation channels, but since it is positive it is likely that the initial excited state is a Σ state since the ground state of CO_2 has Σ symmetry. This near isotropic β suggests that the dissociation is comparable or slower than the rotation of the dissociating CO_2 molecule.

To the authors' knowledge, this is the first time that the CO + O($^3P_{2,1,0}$) product population has been directly observed from the photodissociation of the CO_2 molecule around 13.6 eV using the TSVMI technique. Despite the fact that few theoretical calculations have been performed in this energy region, dissociation information could be retrieved from the kinetic energy release spectra and the product branching electronic, vibrational, and rotational channels of CO could be discerned from the images and used to suggest some general aspects of the dissociation mechanisms.

3.2 Detection of O(^{1}S)

The photofragment yield spectrum of O product from photodissociation of CO_2 is obtained from 13.583 to 13.596 eV by scanning the VUV radiation frequency and gating the O signal in boxcar integrator, as shown in Fig. 4. Only one-color VUV radiation is used for both the photodissociation of CO_2 and the photoionization of the O atom. Interestingly, one diffuse and reproducible peak appears as seen in Fig. 4 that is centered at 109 597 cm^{-1} with FWHM 20 cm^{-1}. This peak probably arises from the resonant excitation of the O fragment followed by its autoionization, since the corresponding CO and CO_2 spectra are relatively flat in this region. Three O transitions are found[18] near 109 597 cm^{-1}, namely $2s^22p^3(^2P^o)4d\ ^1P^o \leftarrow 2s^22p^4\ ^1S$ at 109 591 cm^{-1}, $2s^22p^3(^4S^o)22s\ ^3S^o \leftarrow 2s^22p^4\ ^3P_2$ at 109 589.0 cm^{-1}, and $2s^22p^3(^4S^o)21d\ ^3D^o_{2,1} \leftarrow 2s^22p^4\ ^3P_2$ at 109 589.3 cm^{-1}. Huffman *et al.* pointed out that[19] the $2s^22p^3(^2P^o)4d\ ^1P^o \leftarrow 2s^22p^4\ ^1S$ band at 109 591 cm^{-1} is diffuse in the absorption spectrum, and McGuire[20] calculated this level width as 12.4 cm^{-1}. The peak in Fig. 4 with a 20 cm^{-1} FWHM is in reasonable agreement with the theoretical calculations, so we conclude that this peak is due to a resonant transition followed by autoionization of O(^{1}S).

A time-sliced velocity-mapped O ion image was taken at 109 597 cm^{-1} and the corresponding TKER spectrum is shown in Fig. 5. The signal immediately shows up below 3.9 eV, which matches the threshold for the O(^{1}S) + CO(X $^1\Sigma^+$) channel at 13.589 eV of 3.95 eV fairly well. A progression of bands between 0 and 3.95 eV is in good agreement with the vibrational assignments of CO(X $^1\Sigma^+$) for channel O(^{1}S) + CO(X $^1\Sigma^+$), as shown in Fig. 5(b). These two observations further support the O(^{1}S) autoionization in Fig. 4.

It seems that the spectrum in Fig. 5(b) comprises two parts: four discrete peaks at 3.0–3.9 eV, and a broad feature from 0 eV extending to the CO(X $^1\Sigma^+$) + O(^{1}S) threshold with multiple weak bands on its top. The complexity of this spectrum can be explained by two different dissociation mechanisms in the following paragraph.

The four peaks at 3.0–3.9 eV represent a dissociation channel of the CO(X $^1\Sigma^+$, v = 0–3) + O(^{1}S) productions, with CO(X $^1\Sigma^+$, v = 2) being the dominant population. This highly non-statistical product vibrational distribution implies that when the excited CO_2 is dissociating, the available energy is not randomized among the vibrational degrees of freedom during the time it takes for decomposition. This suggests a rapid dissociation in which the dissociative excited electronic state of CO_2 is highly repulsive. The state that is dissociating is more strongly bent than the ground state because the rotational contours of these peaks are about $\sim$800 cm^{-1}. It is suggested that the dissociation mechanism for these four peaks in Fig. 5(b) is that the excited CO_2 molecule decomposes through a highly repulsive state where the excited molecule is bent. One candidate for this repulsive state is the adiabatic 4 $^1A'$ (ref. 8) that is converging to the CO(X $^1\Sigma^+$) + O(^{1}S) asymptote. Thus, the initially excited Rydberg state must somehow couple to the 4 $^1A'$ state in the exit channel.

The broad peaks from 0 to 4 eV are apparently formed *via* a different dissociation pathway. It is possible that some of the CO_2 molecules in the excited Rydberg state cross over to a different state that dissociates more slowly into the 4 $^1A'$ than the state that produces the observed excess in the lower vibrational levels of CO. The geometry of this state that slowly

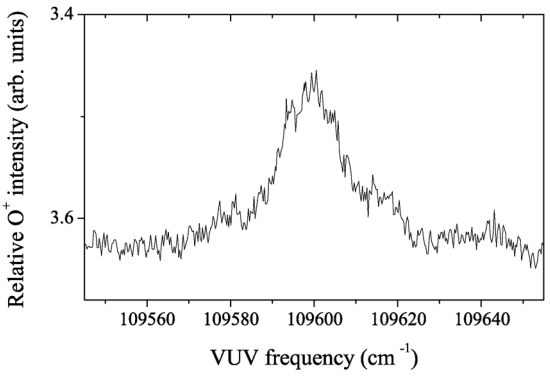

Fig. 4 Photofragment yield spectrum of the O atom from photodissociation of CO_2 as a function of VUV radiation frequency. A single VUV radiation was used for the photodissociation of CO_2 and ionization of the O atom.

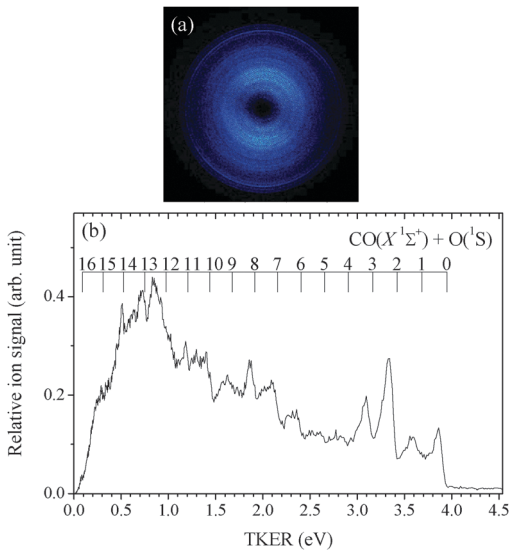

Fig. 5 (a) Time-sliced velocity-mapped raw image of O^+ and (b) total kinetic energy release (TKER) spectrum of the photofragments CO and O from photodissociation of CO_2 at 13.589 eV. The VUV laser was set at 109 596.7 cm^{-1} to coincide with O(^{1}S) transition $2s^22p^3(^2P^o)4d\ ^1P^o \leftarrow 2s^22p^4\ ^1S$.

crosses over to the 4 $^1A'$ is probably close to linear, since most of the rotational states of CO(X $^1\Sigma^+$) are less rotationally excited (<400 cm^{-1}) than the four bands at higher kinetic region, as shown in Fig. 5.

Although in 1972 Lawrence[6] showed that $\sim$30% CO_2 dissociates through a channel that produces CO(X $^1\Sigma^+$) + O(^{1}S) around 90 nm (13.777 eV), to our knowledge there has been no other work reported on this channel in this energy region. In the current study we present for the first time the product distribution of CO(X $^1\Sigma^+$) + O(^{1}S) from photodissociation of CO_2 at 91.24 nm (13.589 eV), as well as two proposed dissociation mechanisms.

3.3 Detection of O(^{1}D)

We have previously reported[7] the photodissociation of CO_2 at O(^{1}D) autoionization line 108 451.5 cm^{-1} and showed for the first time the production of CO(X $^1\Sigma^+$) + O(^{1}D) at this wavelength. Now with the addition of the second VUV radiation, we are able to investigate the O(^{1}D) channels from the photodissociation of CO_2 at different dissociation wavelengths. The probe laser was used to excite the O(^{1}D) autoionization line $2s^22p^3(^2D^o_{3/2})3d\ ^1D^o_2 \leftarrow 2s^22p^4\ ^1D_2$ at 108 451.5 cm^{-1} (13.447 eV) and images were recorded using the TSVMI apparatus at three different dissociation energies at 13.678 eV, 13.605 eV, and 13.568 eV. Three TKER spectra were extracted from the images and are shown in Fig. 6. The O(^{1}D) background signal from photodissociation of CO_2 by the probe laser was checked when the dissociation laser was blocked, and it is ten times smaller than the signal.

In Fig. 6, all the three spectra exhibit a broad feature, peaking around 0.6 eV and extending to the energy region beyond 5 eV. This broad band results from the vibrationally excited CO(X $^1\Sigma^+$) fragment in CO(X $^1\Sigma^+$) + O(^{1}D) channel by the sum-frequency radiation in the dissociation beam, since the extension of the signal to the higher kinetic energy >5 eV matches the maximum available energy of CO(X $^1\Sigma^+$) + O(^{1}D) with sum-frequency photon, as previously shown by Pan *et al.*[7] The assignment of the vibrational states of CO(X $^1\Sigma^+$) at 13.678 eV has been labeled in Fig. 7(b), along with another O(^{1}D) channel that has been assigned to CO(a $^3\Pi$) + O(^{1}D). The kinetic energy distribution of CO(X $^1\Sigma^+$) + O(^{1}D) is highly populated at higher vibrational states of CO(X $^1\Sigma^+$) and decays smoothly to CO(X $^1\Sigma^+$, $v = 0$). The high probability for dissociation into the highly vibrationally excited CO requires that the initially excited Rydberg state crosses over to a state where one of the r_{CO} values is compressed when the other bond is extending and is dissociating. According to Grebenshchikov's calculations,[8] this dissociative state could be the adiabatic X $^1\Sigma_g^+$, degenerate pair $^1\Delta_u/^1\Sigma_u^-$, or 1 $^1\Sigma_g$, since all of the above states correlate to CO(X $^1\Sigma^+$) + O(^{1}D) and they lie below 13 eV.

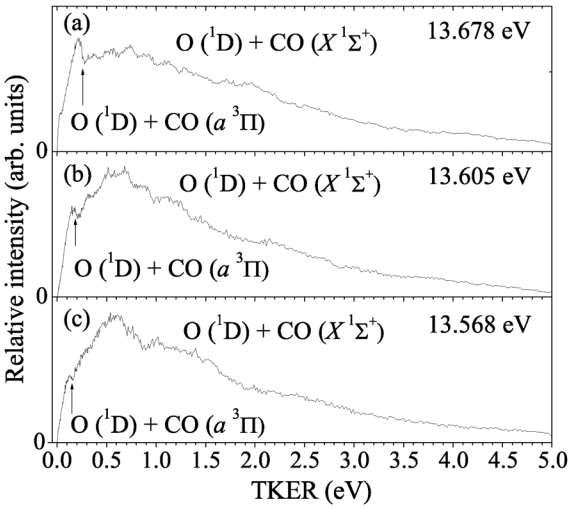

Fig. 6 Total kinetic energy release (TKER) spectra of the photofragments CO and O from photodissociation of the CO_2 molecule at different excitation energies: (a) 13.678 eV; (b) 13.589 eV; (c) 13.568 eV. The probe laser was tuned to 108 451.5 cm^{-1} to coincide with O(^{1}D) autoionization transition $2s^22p^3(^2D^o_{3/2})3d\ ^1D^o_2 \leftarrow 2s^22p^4\ ^1D_2$. The arrows indicate the threshold of CO(a $^3\Pi$) + O(^{1}D) production.

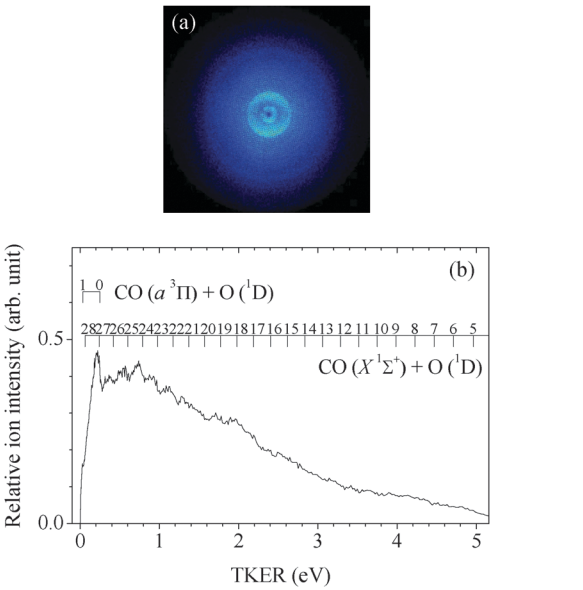

Fig. 7 (a) Time-sliced velocity-mapped raw image of O^+ and (b) total kinetic energy release (TKER) spectrum of the photofragments CO and O from photodissociation of the CO_2 molecule at 13.678 eV. The probe laser was tuned to 108 451.5 cm^{-1} to coincide with O(^{1}D) autoionization transition $2s^22p^3(^2D^o_{3/2})3d\ ^1D^o_2 \leftarrow 2s^22p^4\ ^1D_2$. The arrows indicate the threshold of CO(a $^3\Pi$) + O(^{1}D) production.

In addition to the CO(X $^1\Sigma^+$) + O(^{1}D) channel, there is a small peak in Fig. 6(c) with a threshold that corresponds to CO(a $^3\Pi$) + O(^{1}D) channel. This peak gets more intense as the dissociation wavelength decreases. The image and P(TKER) plot when CO_2 is photolyzed at 13.678 eV are shown in Fig. 7. It is noteworthy that the vibrationally excited CO(a $^3\Pi$, $v = 1$) shows up immediately once the excitation energy exceeds its threshold, as shown by the inner ring in Fig. 7(a) and the small shoulder at 0.03 eV in Fig. 7(b). It is clear that there must be an intersystem crossing between the singlet state that is initially excited and a triplet state that leads to the final observed products. This is the first time that CO(a $^3\Pi$) + O(^{1}D) has been directly observed from photodissociation of CO_2 just above its dissociation threshold.

4 Conclusions

We have investigated the photodissociation of CO_2 in the energy region between 13.540 eV and 13.678 eV using the TSVMI apparatus combined with one- and two-color VUV and UV radiation, by detecting different atomic states of the oxygen fragment. The kinetic energy distributions of several CO_2 dissociation channels have been reported for the first time, including $CO(X\ ^1\Sigma^+) + O(^1D)$, $CO(X\ ^1\Sigma^+) + O(^1S)$, $CO(a\ ^3\Pi) + O(^3P)$, $CO(a\ ^3\Pi) + O(^1D)$, $CO(a'\ ^3\Sigma^+) + O(^3P)$, $CO(d\ ^3\Delta) + O(^3P)$ and $CO(e\ ^3\Sigma^-) + O(^3P)$, in the order of their increasing dissociation energies. Possible dissociation mechanisms have been discussed based on the product vibrational and rotational distributions in the TKER spectra determined from the images. (1) The $CO(a\ ^3\Pi) + O(^3P)$ non-statistical product distribution at 13.540 eV suggests that part of the CO_2 molecules may dissociate very fast so that the available energy could not be randomized among all of the degrees of freedom. (2) For the $CO(X\ ^1\Sigma^+, v = 0–3) + O(^1S)$ non-statistical productions at 13.589 eV, it is possible that the initially excited Rydberg state interacts with the adiabatic $4\ ^1A'$ state which correlates with $CO(X\ ^1\Sigma^+) + O(^1S)$, and this dissociation process is very fast. (3) For the $CO(X\ ^1\Sigma^+, v = 0–16) + O(^1S)$ broad feature in the TKER spectrum at 13.589 eV, some of CO_2 in the excited Rydberg state may couple to a different state that dissociates more slowly into the $4\ ^1A'$ state, and finally $CO(X\ ^1\Sigma^+) + O(^1S)$ products. (4) For $CO(X\ ^1\Sigma^+) + O(^1D)$ dissociation channel at 13.568–13.678 eV, the initially excited Rydberg state may cross over to a state where one of the C–O bonds of CO_2 is compressed while the other one is extending and dissociating. Most of the above mentioned excited dissociative states could be possibly identified with help from a previous high-level *ab initio* calculation.[8,9]

Acknowledgements

Yu Song, Hong Gao, and William M. Jackson gratefully acknowledge the support of the Chemical Structure, Dynamics and Mechanism-A Program (CSDM-A) under NSF grant CHE-0957872. Hong Gao, Yih Chung Chang, Zhou Lu and C. Y. Ng also acknowledge the support of the Chemical Sciences, Geosciences and Biosciences Division, Office of Basic Energy Sciences, Office of Science, U.S. Department of Energy, under Contract No. DE-FG02-02ER15306. William M. Jackson gratefully acknowledges the support of Alexander von Humboldt foundation and thanks Sergy Yu. Grebenshchikov at the Technical University of Munich for the many discussions that he had with him.

References

1 Y. L. Yung and W. B. DeMore, *Photochemistry of Planetary Atmospheres*, Oxford University Press, New York, 1999.
2 W. Chan, G. Cooper and C. Brion, *Chem. Phys.*, 1993, **178**, 401–413.
3 G. M. Lawrence, *J. Chem. Phys.*, 1972, **56**, 3435–3442.
4 K. P. Huber and G. Herzberg, Constants of Diatomic Molecules, (data prepared by J. W. Gallagher and R. D. Johnson, III), NIST Chemistry WebBook, NIST Standard Reference Database Number 69, National Institute of Standards and Technology, Gaithersburg MD, 20899, http://webbook.nist.gov.
5 D. L. Judge and L. C. Lee, *J. Chem. Phys.*, 1973, **58**, 104–107.
6 G. M. Lawrence, *J. Chem. Phys.*, 1972, **57**, 5616–5617.
7 Y. Pan, H. Gao, L. Yang, J. Zhou, C. Y. Ng and W. M. Jackson, *J. Chem. Phys.*, 2011, **135**, 071101.
8 S. Y. Grebenshchikov, *J. Chem. Phys.*, 2013, **138**, 224106.
9 S. Y. Grebenshchikov, *J. Chem. Phys.*, 2013, **138**, 224107.
10 K. Yoshino, J. Esmond, Y. Sun, W. Parkinson, K. Ito and T. Matsui, *J. Quant. Spectrosc. Radiat. Transfer*, 1996, **55**, 53–60.
11 J. Zhou, K.-C. Lau, E. Hassanein, H. Xu, S.-X. Tian, B. Jones and C. Y. Ng, *J. Chem. Phys.*, 2006, **124**, 034309.
12 Y. Song, H. Gao, C. Ng and W. Jackson, *EAS Publ. Ser.*, 2012, **58**, 295–299.
13 H. Gao, Y. Song, W. M. Jackson and C. Y. Ng, *J. Chem. Phys.*, 2013, **138**, 191102.
14 R. Mahon and F. Tomkins, *IEEE J. Quantum Electron.*, 1982, **18**, 913–920.
15 R. Hilbig and R. Wallenstein, *IEEE J. Quantum Electron.*, 1983, **19**, 194–201.
16 A. G. Suits, *Acc. Chem. Res.*, 2008, **41**, 873–881.
17 D. J. Bamford, M. J. Dyer and W. K. Bischel, *Phys. Rev. A: At., Mol., Opt. Phys.*, 1987, **36**, 3497–3500.
18 A. Kramida, Yu. Ralchenko, J. Reader and NIST ASD Team, *NIST Atomic Spectra Database (version 5.1)*, National Institute of Standards and Technology, Gaithersburg, MD, 2013.
19 R. E. Huffman, J. C. Larrabee and Y. Tanaka, *J. Chem. Phys.*, 1967, **47**, 4462–4471.
20 E. J. McGuire, *Phys. Rev. A: At., Mol., Opt. Phys.*, 1979, **19**, 1978–1998.